

Article

Electrodialytic Energy Storage System: Permselectivity, Stack Measurements and Life-Cycle Analysis

Kjersti Wergeland Krakhella ^{1,2}, Marjorie Morales ^{2,3}, Robert Bock ², Frode Seland ¹ and Odne Stokke Burheim ^{2,*} and Kristian Etienne Einarsrud ¹

¹ Department of Materials Science and Engineering, Norwegian University of Science and Technology (NTNU), NO-7491 Trondheim, Norway; kjerskra@gmail.com (K.W.K.); frode.seland@ntnu.no (F.S.); kristian.e.einarsrud@ntnu.no (K.E.E.)

² Department of Energy and Process Engineering, Norwegian University of Science and Technology (NTNU), NO-7491 Trondheim, Norway; marjorie.morales@ntnu.no (M.M.); robert.bock@ntnu.no (R.B.)

³ INRIA BIOCORE, BP 93, CEDEX 06902 Sophia Antipolis, France

* Correspondence: burheim@ntnu.no

Received: 22 January 2020; Accepted: 3 March 2020; Published: 7 March 2020



Abstract: Reverse electro dialysis and electro dialysis can be combined into a closed energy storage system, allowing for storing surplus energy through a salinity difference between two solutions. A closed system benefits from simple temperature control, the ability to use higher salt concentrations and mitigation of membrane fouling. In this work, the permselectivity of two membranes from Fumatech, FAS-50 and FKS-50, is found to be ranging from 0.7 to 0.5 and from 0.8 to 0.7 respectively. The maximum unit cell open-circuit voltage was measured to be 115 ± 9 mV and 118 ± 8 mV at 25 °C and 40 °C, respectively, and the power density was found to be 1.5 ± 0.2 W m_{uc}⁻² at 25 °C and 2.0 ± 0.3 W m_{uc}⁻² at 40 °C. Given a lifetime of 10 years, three hours of operation per day and 3% downtime, the membrane price can be 2.5 ± 0.3 \$ m⁻² and 1.4 ± 0.2 \$ m⁻² to match the energy price in the EU and the USA, respectively. A life-cycle analysis was conducted for a storage capacity of 1 GWh and 2 h of discharging. The global warming impact is $4.53 \cdot 10^5$ kg CO₂ equivalents/MWh and the cumulative energy demand is $1.61 \cdot 10^3$ MWh/MWh, which are 30% and 2 times higher than a lithium-ion battery pack with equivalent capacity, respectively. An electro dialytic energy storage system reaches a comparable global warming impact and a lower cumulative energy demand than a lithium-ion battery for an average life span of 20 and 3 years, respectively.

Keywords: electro dialytic energy storage system (EESS); reverse electro dialysis (RED); permselectivity; life-cycle analysis (LCA)

1. Introduction

The prognosis for 2050 of the world's electricity production done by DNV-GL [1] shows that over 63% of the production will stem from renewable sources like wind and solar power. These energy sources are intermittent and often not available when and where we need energy, making a renewable-based economy dependent on energy storage.

Examples of ways to store energy are with hydrogen, lithium-ion batteries, capacitors and phase change materials where each storage system has its niche, e.g., cheap, long-lived, high power or high efficiency. A potential storage system which is cheap, easy to scale and chemically flexible is storage by salinity gradients. The available energy when one cubic meter of river water enters the sea is 2.3 MJ [2,3], corresponding to a water column of over 200 m [4]. Using brine and river water instead gives us 15 MJ of available energy, which is equivalent to the volumetric energy density of hydrogen at 3 bar.

An energy storage system based on salinity gradients combines a desalination technology with a mixing technology. The system is charged with external power increasing the concentration difference between two solutions, and energy is stored in the form of a chemical potential difference. The system is discharged by mixing the two solutions, converting the chemical potential to electricity and decreasing the concentration difference. The very same system can also be charged using waste-heat and has hydrogen as output [5,6]. An illustration of a general energy storage system with solutions of different concentrations is given in Figure 1.

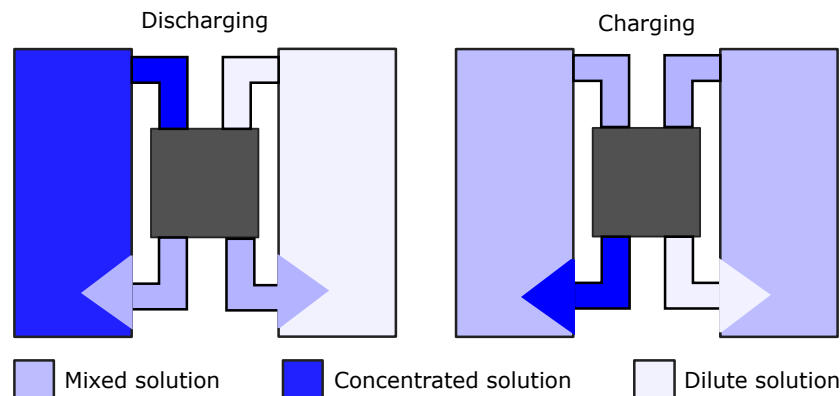


Figure 1. Illustration of an energy storage system: discharging (left) by mixing the solutions and charging (right) by increasing the concentration difference.

Examples of combinations of technologies which together make up a salinity gradient energy storage system (SGESS) are reverse electrodialysis (RED) and electrodialysis (ED), pressure-retarded osmosis (PRO) and reverse osmosis (RO), and capacitive Donnan potential (CDP) and membrane capacitive deionisation (MCDI). A model comparing these SGESSs is carried out by Jalili et al. [7], where RED/ED and PRO/RO were preferred over CDP/MCDI, and at higher temperatures, RED/ED had the highest power density and efficiency. This work is based on these findings and focuses on the electrodiolytic energy storage system (EESS) based on RED and ED.

An EESS was first suggested by Kingsbury et al. in 2015 [8]. Kingsbury modelled and did experiments on an EESS using concentrations in the range of naturally occurring concentrations (0.25 mol/kg and 0.5 mol/kg), where the solutions were circulated in the cell stack during the experiment. The round-trip efficiency was measured to a maximum of 34% and the power density was found to be from 0.07 to 0.44 W m⁻². Egmond et al. [9] later conducted experiments and modelled an EESS at elevated temperature (40 °C). The solution concentrations were close to naturally occurring concentrations (0.02 mol/kg and 0.85 mol/kg) and were circulated in the cell stack (like Kingsbury et al. [8]). Egmond found that the ohmic resistance was relatively constant throughout the concentration difference range except at the highest difference due to high resistance in the dilute compartment. By increasing the temperature, the ohmic resistance decreased, which increased the power density, while the net water transport through the membrane increased with temperature, lowering the power density. The net effect on efficiency was that increasing the temperature increased the EESS efficiency.

Both Kingsbury et al. and Egmond et al. circulated the solutions and used constant currents. In our study, the concentration of the solutions is kept constant while controlling the potential and measuring the current with concentration close to saturation point of the NaCl (6 M) to increase the chemical potential. Polarisation curves give information regarding kinetics in EESS and an energy storage efficiency based on realistic operating current densities. By keeping both the inlet concentrations constant while measuring polarisation curves, we can get a better understanding of the limiting kinetics. The polarisation curve will also give the ideal discharging current for maximum power density, and using a realistic current restriction (e.g., the duck curve constraint explained in Jalili et al. [7]), the charging current can be calculated, together with the total efficiency of the EESS.

The power output from an EESS is highly dependent on the concentration difference between the two solutions [8,9], where higher difference results in higher power density. However, the membranes available for an EESS are mostly used for naturally occurring concentrations and salts (seawater and river water) [10], while higher concentrations are relevant for a closed system.

This paper will compare the performance of EESS at two temperatures, where the power density and efficiency are chosen as parameters describing the performance. The permselectivity is measured for two relevant membranes at higher salt concentrations. Both stack measurements and permselectivity are compared with theoretically expected values. The results also include a brief life-cycle analysis (LCA) of the EESS.

2. Theory

A schematic of the EESS while discharging is shown in Figure 2. In the discharging process, the chloride ions travel from the concentrated solution to the dilute solution through the anion exchange membrane (AEM), while the sodium ions travel from the concentrated solution to the dilute solution through the cation exchange membrane (CEM). At each electrode, a redox or rinse solution is circulated. For the experiments carried out in this project, iron(II/III)chloride is used as a redox solution.

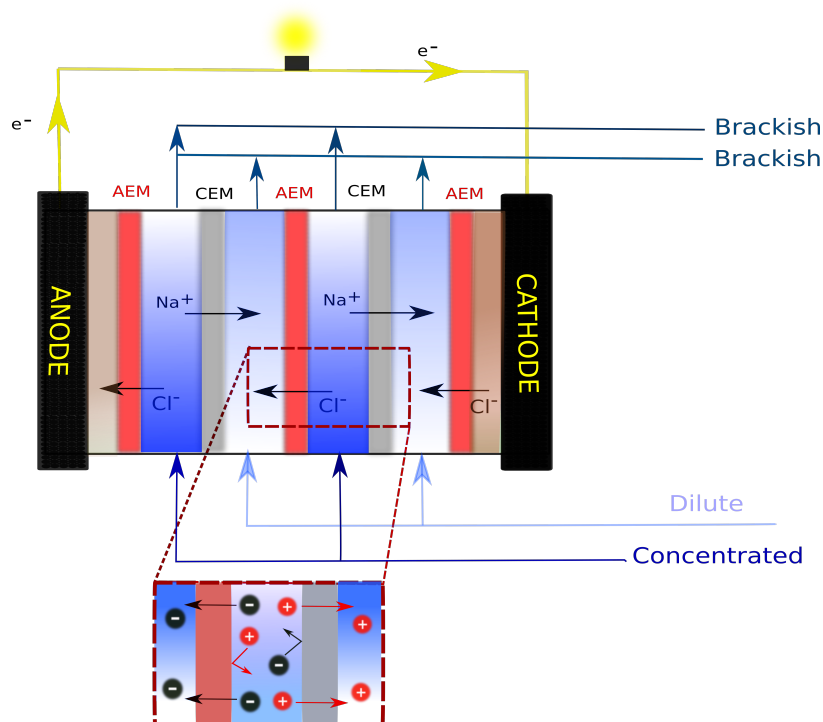


Figure 2. The figure shows the discharging process of an Electrodeionization energy storage system (EESS). The sodium and chloride ions travel from the concentrated solutions to the dilute solutions, through cation exchange membranes (CEMs) and anion exchange membranes (AEMs), respectively. At both electrodes, iron(II/III)chloride is circulated. Chloride ions are absorbed by the redox solution at the anode and released from the redox solution at the cathode.

During discharge, the chloride ions enter the redox solution at the anode, while at the cathode, chloride ions leave the redox solution. The reactions at each electrode are as follows:



The electrons conduct from the anode to the cathode while discharging. When the EESS is charging, electrons are forced in the opposite direction using an external power source.

The open-circuit voltage (OCV) over a unit cell is derived from the Nernst equation:

$$E_{\text{OCV}} = 2\bar{\alpha} \frac{RT}{zF} \ln \left(\frac{c_c \gamma_c}{c_d \gamma_d} \right), \quad (2)$$

where R is the ideal gas constant, T is the temperature in Kelvin, F is the Faraday constant, z is the valence number and $\bar{\alpha}$ is the arithmetic mean of the permselectivities of the CEM and AEM. The permselectivity of the membranes expresses the capability to discriminate between two ions with different charge. It is highly dependent on solution concentration and transport number of salt and water but less dependent on solution temperature [10]. c_c and c_d , and γ_c and γ_d are the molarity and activity coefficients of the concentrated and dilute solution, respectively.

The apparent permselectivity is here defined as the measured cell potential, with zero concentration gradient and zero flux of water and charge, divided by the theoretical EMF (chemical potential divided by Faraday constant). The effective permselectivity is here defined as the observed/measured open cell potential in a process where solutions flow through the cell and concentration layers build up due to osmosis and migration, divided by the theoretical EMF [11]. The apparent cell potential does not include osmotic water transport but accounts for the electroosmotic drag (t_w) as this coupling directly affects the open cell potential as described in Equation (3). The effective permselectivity is affected by osmosis of water in the sense that water diffuses from the dilute to the concentrate solution and lowers the concentration difference; this changes as water flows through the cell (adjacent to the membranes) at different velocities. It also changes as the current density changes because of boundary layer diffusion phenomena. The co-transport of water due to electroosmosis is water carried as a hydration shell around the counterions and co-ions (hydration number). Given a higher flux of counterions than co-ions, the water transported due to electroosmosis will flow from the concentrated to the dilute solution, thus increasing the permselectivity. The permselectivity for an ion exchange membrane (IEM) is given in Equations (3) and (4) (modified from Reference [10] to be valid for concentrations higher than 0.6 M; see Appendix A for a detailed derivation):

$$\alpha = t_s - t_w M_w \frac{\Delta m_s}{\Delta \ln(m_s \gamma_s)} \quad \text{for } m_1 \neq m_2 \quad (3)$$

$$\alpha = t_s - t_w M_w m_s \quad \text{for } m_1 = m_2 \quad (4)$$

where t_s and t_w are the transport numbers of salt and water respectively, M_w is the molar weight of water ($0.018 \text{ kg mol}^{-1}$), m_s is the molality of the salt solution and Δm_s is the difference in molality of the solutions on each side of the membrane. Given the constant transport numbers of salt and water, the permselectivity would increase with concentration difference.

The transport number of salt is defined as the amount of the current carried by the counterion. If more co-ions are transported with the salt gradient, the transport numbers decrease, and the amount of co-ions in the membrane is dependent on the salt concentration in the bulk and the concentration of the fixed charges in the membrane [12]. FAS-50 and FKS-50 have averages of 0.13 mol and 0.10 mol fixed charges per square meter membrane, respectively [13,14].

Zlotorowicz et al. [10] measured the transport number of water and salt in the membranes FAD-PET-75 and FKD-PET-75 from Fumatech at a concentration up to 0.6 M, where the transport numbers of salt were 0.93 and 0.998 for CEM and AEM, respectively. Długołęcki et al. [15] modelled the transport number of salt in the same membranes as used by Zlotorowicz et al., where linear regression gives the following salt transport numbers for FKS and FAD from Fumatech:

$$\begin{aligned} t_s^{\text{AEM}} &= -0.09 c + 1 \\ t_s^{\text{CEM}} &= -0.03 c + 1 \end{aligned} \quad (5)$$

where c is the molarity of the solution. In this study, c is the arithmetic mean of the concentrations on each side of the membranes, which is $c = 2.525$ M for all our cases.

The water transport number is dependent on osmotic and electroosmotic effects [16]. The osmotic effect will be higher with larger concentration differences, while the number of water molecules per ion is lowered with concentration [17]. Zlotorowicz et al. [10] measured the transport number of water to be 8 and 6 for CEM and AEM, respectively. However, due to the large difference between the concentrations in the present work and the concentrations used by Zlotorowicz et al., the water transport number in AEM and CEM for the model is varied between 0 and 10 [18]. The permselectivity, given salt transport number equal to Equation (5), average water transport number: $t_w = 5$ and activity coefficients following Equation (6), is plotted in Figure 3.

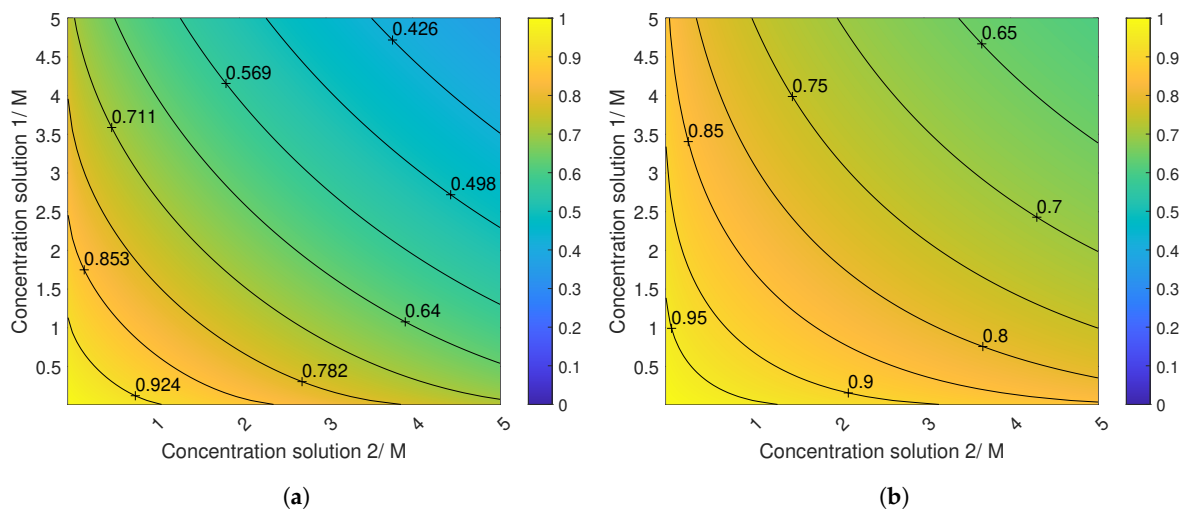


Figure 3. Permselectivity for AEM (a) and CEM (b) calculated with Equation (3): $t_w = 5$, t_s follows Equation (5), with the membrane concentration equal to the average concentration between the solutions and activity coefficients following Equation (6). Values on the diagonal of equal concentrations are interpolated and do not show the correct values obtained with Equation (4).

Fumatech reports a permselectivity of 0.97–0.99 and 0.92–0.96 for FKS-50 and FAS-50 respectively [13,14] at 25 °C and 0.5 M NaCl.

Activity coefficients for solutions with higher concentrations than 1 M lie beyond Debye–Hückel, Davies and Truesdell–Jones model limitations. Stokes and Robinsons equation is therefore used [19,20]:

$$\gamma_{\pm} = \exp \left(\frac{Az_{\pm}^2 \sqrt{I}}{1 + Ba \sqrt{I}} - \frac{h}{\nu} \ln(a_w) - \ln(|1 + (M_w(\nu - h)m)|) \right) \quad (6)$$

where I is the ionic strength, with 1 mol kg⁻¹ as reference; z_{\pm} is the mean of the valence of the cation and anion (1 for NaCl); ν is the number of ions per molecule (2 for NaCl); h is the hydration number of NaCl; and a is the distance of the closest approach (the minimum distance between the center core of two particles before it is reflected back). h and a are found to be 5.2 and 0.42 nm respectively from curve fitting to Reference [21]. The hydration number and the distance of the closest approach is found to depend on temperature and concentration [17]; however this is not taken into consideration for the modelling in this work. A and B are temperature dependent and given in Equation (7) ($A = 1.18$ (kg/mol)^{1/2} and $B = 3.29 \cdot 10^9$ (kg/mol)^{1/2} m⁻¹ at 25 °C [22]):

$$A = (2\pi N_A \rho_w)^{1/2} \left(\frac{e^2}{4\pi \epsilon_0 \epsilon_{r,w} k_B T} \right)^{3/2} \quad (7)$$

$$B = e \left(\frac{2N_A \rho_w}{\epsilon_0 \epsilon_{r,w} k_B T} \right)^{1/2},$$

where N_A is Avogadro's number, ρ_A is the density of the solvent (for simplicity, set to 1000 kg m^{-3}), e is the elementary charge, ϵ_0 is permittivity of vacuum and k_B is Boltzmann constant. $\epsilon_{r,w}$ is the dielectric constant of the solvent [23] (here, water) and given in Equation (8) (rewritten to use Kelvin instead of Celsius):

$$\epsilon_{r,w} = 87.74 - 0.4008 \cdot (T - 273.2) + 9.398 \cdot 10^{-4} \cdot (T - 273.2)^2 - 1.410 \cdot 10^{-6} \cdot (T - 273.2)^3 \quad (8)$$

In Equation (6), a_w is the water activity as a function of the salt concentration given in Equation (9) [24]:

$$\begin{aligned} a_w &= \gamma_w x_w \\ \gamma_w &= \exp(\alpha_{a_w, \text{NaCl}} x_s^2 + \beta_{a_w, \text{NaCl}} x_s^3) \\ x_s &= \frac{m}{m + 1/M_w} \\ x_w &= \frac{1/M_w}{m + 1/M_w} \end{aligned} \quad (9)$$

where γ_w is the activity constant of water (equal to 1 with no salt present), x_w is the mole fraction of water, $\alpha_{a_w, \text{NaCl}}$ and $\beta_{a_w, \text{NaCl}}$ are constants found from Miyawaki to be 1.825 and -20.78 for NaCl respectively [24]. x_s is the mole fraction of salt.

The modelled activity coefficient from the Stokes–Robinson equation (Equation (6)) is plotted in Figure 4 together with the data from Pytkowicz [21]. One reason for the deviation between the Stokes–Robinson equation and the measured activity coefficient of NaCl is the assumption of no temperature or concentration dependency in the modelled hydration number. Afanasiev et al. [25] suggest an exponential dependence on concentration and negligible dependency of temperature, while Onori [26] gives a linear dependence on concentration and states that the hydration number increases with temperature. For simplicity, neither the dependence on temperature nor concentration of the hydration number nor the distance of the closest approach is taken into consideration for this work.

Increasing the solution activity difference between the two solutions in the EESS will increase the OCV and thereby the power density. From the activity coefficient perspective, it is beneficial to have one concentration close to 1 M and the other concentration at 0 M or 5 M. The activity also increases with increasing temperature, but the impact is less prominent than for concentration.

The total unit cell voltage is given in Equation (10) for charging and in Equation (11) for discharging.

$$E^{\text{charging}} = E_{\text{OCV}} + r_{\Omega} i^{\text{charging}} \quad (10)$$

$$E^{\text{discharging}} = E_{\text{OCV}} - r_{\Omega} i^{\text{discharging}} \quad (11)$$

where i is the current density per cross-sectional area and r_{Ω} is the ohmic resistance ($\Omega \text{ m}^2$) of a unit cell. The latter is the sum of the resistance of one AEM, one CEM, one compartment of dilute and one compartment of concentrated solution. It is important to emphasise that the electrode resistance, $r_{\text{electrode}}$, can be assumed negligible for a stack containing a large number of unit cells [27]. However, on the laboratory scale (fewer or single unit cells), the electrode resistance needs to be considered. The ohmic resistance in one unit cell is given in Equation (12) [28]:

$$r_{\Omega} = \frac{\delta_m}{\sigma_{\text{AEM}}(1 - \beta)} + \frac{\delta_m}{\sigma_{\text{CEM}}(1 - \beta)} + \frac{\delta_s}{\sigma_d \epsilon^2} + \frac{\delta_s}{\sigma_c \epsilon^2} \quad (12)$$

where δ_m is the membrane thickness, σ_{AEM} and σ_{CEM} are the ionic conductivities in the AEM and CEM (S m^{-1}) respectively and β (dimensionless) is the spacer shadow effect [29] or the part of the membrane that is covered by a spacer. δ_s is the thickness of the spacer, and ϵ (dimensionless) is the porosity or the factor to correct for the occupied volume by the spacer (equal to 1 with no spacer). The porosity is defined as one minus the volumetric ratio (the ratio of the apparent gravity and the specific gravity of the spacer, see [28]) and squared to represent the tortuous behavior of the ion transport

in the spacer-filled channel. σ_d and σ_c are the conductivity of the dilute and concentrated solution respectively ($S m^{-1}$). Theoretical values are deduced from conductivity measurements of NaCl in water at 25 °C from [30] (wt% to $mol L^{-1}$ and $\mu S cm^{-1}$ to $S m^{-1}$) and fit to Kohlrausch's equation given in Reference [31] (p. 22):

$$\begin{aligned}\sigma_{sol,25} &= k_1c - k_2c^{3/2} \\ k_1 &= 11.8 \pm 0.2 S m^{-1} \\ k_2 &= 2.7 \pm 0.1 S/(mol m^{-1})^{1/2}\end{aligned}\quad (13)$$

where $\sigma_{sol,25}$ is the solution conductivity at 25 °C ($S m^{-1}$). The theoretical temperature effect on the resistance is based on data from Schlumberger [32]:

$$\rho_{sol} = \frac{1}{\sigma_{sol,25}} \frac{46.5 \text{ } ^\circ C}{T + 21.5 \text{ } ^\circ C} \quad (14)$$

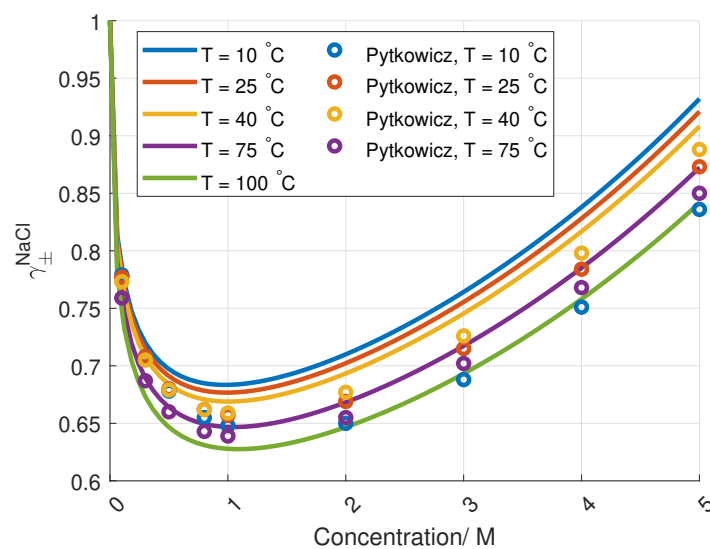


Figure 4. Modelled activity coefficient for NaCl for different concentrations and temperatures, together with data from Pytkowicz [21]: The model follows the Stokes–Robinson equation, where a and h are found from curve fitting to data from Reference [21].

The temperature T has the the unit °C.

The power density per unit cell (uc) area, P ($W m_{uc}^{-2}$), is the electrode voltage (per unit cell, AEM and CEM), E (V) from Equation (11), multiplied by the current density, i ($A m^{-2}$):

$$P_{uc}^{charging} = E_{OCV}i^{charging} + r_{\Omega}(i^{charging})^2 \quad (15)$$

$$P_{uc}^{discharging} = E_{OCV}i^{discharging} - r_{\Omega}(i^{discharging})^2 \quad (16)$$

Following the duck curve constraint (see Jalili et al. [7]), the current density while charging is approximately half the current density while discharging.

The efficiency of discharging the EESS is the net power density produced, where power used for pumping is subtracted, divided by the reversible power density. The efficiency of charging is the reversible power density divided by the power density used by ED and the power used for pumping. The equations of the current density, power losses in pumping and the EESS efficiency can be found in Jalili et al. [7]. Given no pumping losses and purely ohmic losses, the power density per unit cell (uc) area, P ($W m_{uc}^{-2}$), is the electrode voltage (per unit cell, AEM and CEM), E (V) Equation (11),

multiplied by the current density, i ($A\ m^{-2}$), and discharging is 0.8 and 0.5 respectively; the total efficiency of the EESS is 0.4 [7].

2.1. Life-Cycle Analysis

Life-cycle analysis is a valuable technique for targeting the environmental impacts associated with a product and can be very useful for assessing emerging technologies, providing environmental guidance at an early stage of development [33]. Two ISO standards (ISO 14040 and 14044) describe the framework and principle for conducting an LCA. There are four phases: (i) goal and scope definition, (ii) life-cycle inventory compilation, (iii) life-cycle impact assessment and (iv) interpretation of results.

2.1.1. Goal, Scope and Boundaries Definition

This study aims to perform the environmental profile associated with the production of a full-scale EESS system. A cradle-to-gate assessment was performed, which is the analysis of a partial product life cycle from resource extraction (cradle) to the factory gate, i.e., focusing in the manufacturing stage, before the transportation to the consumer. The functional unit chosen was 1 MWh of energy storage. The system boundary includes the production of the material used in the manufacturing of EESS, considering its transports, energy, infrastructure, equipment and emissions associated.

2.1.2. Life-Cycle Inventory Compilation and Data Quality

Life-cycle inventory (LCI) data is provided by primary data obtained in experiments from the RED-stack. Background data from Ecoinvent v3.4 database was used for upstream processes, such as material and electricity production. For the LCA, the Cut-off U system was used. This system implies that the impact for producing a product is allocated to the first user, and potential recycling of the product does not benefit the LCA [34]. Using the cut-off system also implies that any use of recycled materials in the production only includes the impact of the recycling process and not the impact of the production of materials itself. The LCI data is shown in Section 4, with details on the total mass of each material needed for building a full-scale EESS.

2.1.3. Life-Cycle Impact Assessment

The life-cycle assessment considers the potential environmental impact assessment of the full-scale EESS system. Two impact categories were evaluated: global warming potential (GW) and cumulative energy demand (CED). The CED quantifies the primary energy (in MWh) required in the production of an EESS system. The GW refers to those emissions contributing to global warming, such as CO_2 , CH_4 and N_2O , measured in kg CO_2 equivalent [35]. The software SimaPro v8.3 is used for the LCA, where the characterisation factors from the midpoint (H) ReCiPe 2016 method v1.1 [36] and CED method v1.10 [37] were used for determining GW and CED, respectively.

3. Methodology

The maximum concentration in the experiments was set to 5.0 M, even though the solubility limit of NaCl is 6 M, to avoid possible precipitation of salt. The dilute solution starts at 0.05 M due to high ohmic resistance at lower concentrations [7] resulting in a drop in power density (see Equation (16)). When the EESS is fully discharged, both the solutions are at 2.525 M (the average concentrations is always 2.525 M). Experiments and the model are run with the solution temperature at both 25 °C and 40 °C, and the material and cell properties are given in Table 1. The model does not account for losses due to concentration polarisation, and stability analysis regarding time and ageing of the system is not taken into consideration.

Table 1. Materials and cell properties for the cell stack used in the experiments and in the modeling.

Name	Symbol	Value
Solutions		
Flow salt solution	$\Phi_{\text{solutions}}$	7.0 mL min ⁻¹
Flow redox solution	Φ_{redox}	7.0 mL min ⁻¹
Flow salt solution ($\Phi / (60 \cdot 10^6 \cdot \delta_s \cdot w \cdot \epsilon)$)	$v_{\text{solutions}}$	0.0012 m s ⁻¹
Flow redox solution ($\Phi / (60 \cdot 10^6 \cdot \delta_s \cdot w \cdot \epsilon)$)	v_{redox}	0.011 m s ⁻¹
Concentration dilute solution	c_d	0.05–2.525 M
Concentration concentrated solution ($c_c = 5.05 - c_d$)	c_c	5.0–2.525 M
Temperature	T	[297, 313] K
Dielectric constant ($T = [297, 313]$ K)	τ_w	[78.4, 73.2] [23]
Resistance		
Resistance AEM	R_{AEM}	$1.44 \cdot 10^{-4} \Omega \text{ m}^2$ [14]
Resistance CEM	R_{CEM}	$1.00 \cdot 10^{-4} \Omega \text{ m}^2$ [13]
Cell geometry		
Channel thickness	δ_s	$1.55 \cdot 10^{-4} \text{ m}^*$
Channel width	w	$4.0 \cdot 10^{-2} \text{ m}^*$
Channel length	l	$9.0 \cdot 10^{-2} \text{ m}^*$
Membrane thickness	δ_m	$5.0 \cdot 10^{-5} \text{ m}^*$
Area space and membrane	A_{tot}	130 mm · 90 mm [38]
Effective area membrane	A_m	90 mm · 60 mm [38]
Spacer parameters		
Open area	OA	0.65 **
Thread thickness	δ_t	$8.0 \cdot 10^{-5} \text{ m}^{**}$
Mesh opening	δ_o	$3.37 \cdot 10^{-4} \text{ m}^{**}$
Maximum spacer shadow ($1 - OA$)	β	0.35 ***
Specific gravity (polyester)	SG_{poly}	1380 kg m^{-3} [39]
Weight fabric	m_{spacer}	0.0333 kg m^{-2} *
Apparent gravity	AG_{spacer}	214.6 kg m^{-3} ***
Porosity ($1 - AG_{\text{poly}} / SG_{\text{poly}}$)	ϵ	0.844 ***

* measured, ** in correspondence with Fumatech, *** calculated.

3.1. Membranes

The membranes used in the stack measurements and the measurements of the permselectivity were FAS-50 and FKS-50, delivered wet in an ED-40 stack from Fumatech. The membranes were chosen due to their high permselectivity, low area resistance and relatively low price [13,14]. At the same time, the membranes were requested to have a certain mechanical strength to not break when pressure was added. Their specification are given in Table 2.

Table 2. Membrane properties.

Properties	FAS-50	FKS-50
Type	Anion Exchange Membrane	Cation Exchange Membrane
Thickness	45–55 μm	45–55 μm
Specific Area Resistance	0.6–1.5 (in Cl ⁻ form) $\Omega \text{ cm}^2$	1.8–2.5 (in Na ⁺ form) $\Omega \text{ cm}^2$
Specific Conductivity	3–8 (in Cl ⁻ form) mS cm^{-1}	2.0–3.0 (in Na ⁺ form) mS cm^{-1}
Ion Exchange Capacity	1.6–2.0 (in Cl ⁻ form) meq g^{-1}	1.2–1.4 (in Na ⁺ form) meq g^{-1}
Selectivity	92–96%	97–99%
Swelling	0–1% (H ₂ O at 25 °C)	0% (H ₂ O at 25 °C)

The cell contained NaCl solution; thus, the membranes were already ion-exchanged to Na^+ and Cl^- ions. Before stack measurements, the correct concentrations were pumped through the flow compartments until a stable OCV was obtained. The same membranes were later used to measure the permselectivity, where the membranes were stored in a NaCl solution for minimum one week before the permselectivity was measured.

3.2. Permselectivity Measurements

The membrane was placed between two solutions with different concentrations, where rubber rings on each side of the membrane prevented leaking. The solution was stirred throughout the experiment with magnetic stirrers. An agar/3 M KCl salt bridge, half-filled with the solutions from the glass containers, connected the glass containers with a saturated KCl solution. Two double junction Ag/AgCl electrodes with the 3 M KCl solution were set in the saturated KCl solution at the end of the salt bridge. The setup can be seen in Figure 5.

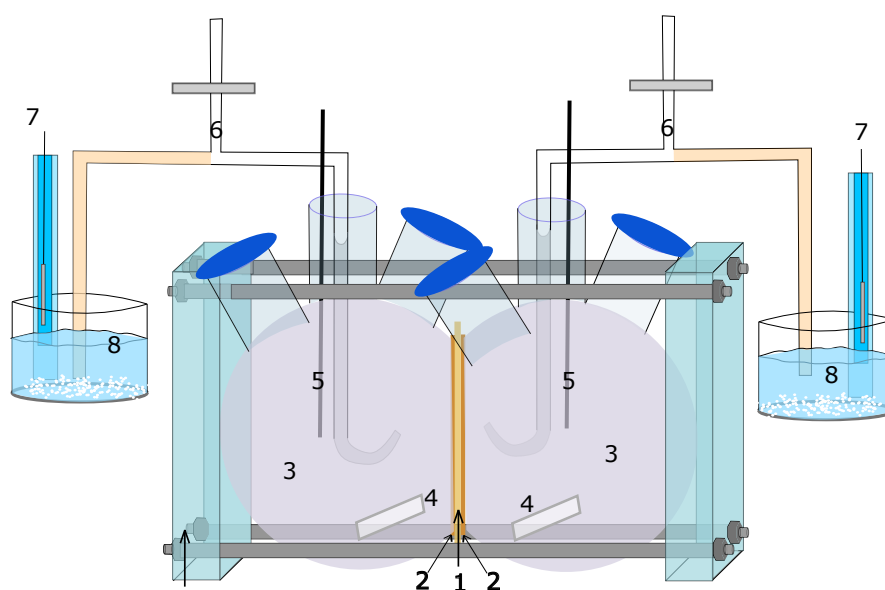


Figure 5. The setup used for the permselectivity measurements: In the figure (1) is the membrane; (2) is the sealing rings; (3) is the glass containers, one with dilute solution and one with concentrated solution; (4) is the magnets for stirring; (5) is the thermometers; (6) is the Agar/KCl salt bridges; (7) is the double junction Ag/AgCl reference electrodes; and (8) is saturated KCl solutions.

The OCV was measured for a minimum of one hour using a Gamry Interface 5000E potentiostat. The permselectivity was found by dividing the measured OCV by the calculated OCV given in Equation (2) (with $\alpha = 1$).

Each membrane (FAS-50 and FKS-50) was measured with each pair of concentrations: 5.000 M/0.05000 M, 4.500 M/0.5500 M, 3.000 M/2.050 M and 2.525 M/2.525 M. The same concentrations used in the stack experiments were also used in the permselectivity measurements, with one exception: The stack measurement carried out with solutions of equal concentration (2.525 M) had a calculated OCV of 0 V, making the calculation of the permselectivity invalid. The concentrations were set to 2.525 M and 2.800 M instead.

3.3. Stack Measurements

The cell used for stack measurements was a Fumatech ED-40 cell. The stack contains membranes (FAS-50 and FKS-50), spacers (polyester) and gaskets (PVC), in addition to two electrodes (titanium and iridium plasma coated stainless steel) [38]. The electrodes are very robust and made for much more intense chemistry (low pH and higher half cell potential). The electrodes were chosen for their very high stability and a strong catalyst for oxygen evolution. In the longer term, other electrodes and electrode improvements are topics for investigation—as for the entire RED and ED systems [40]. All the layers are pressed together by two end plates of PEEK. An illustration of the setup is shown in Figure 6.

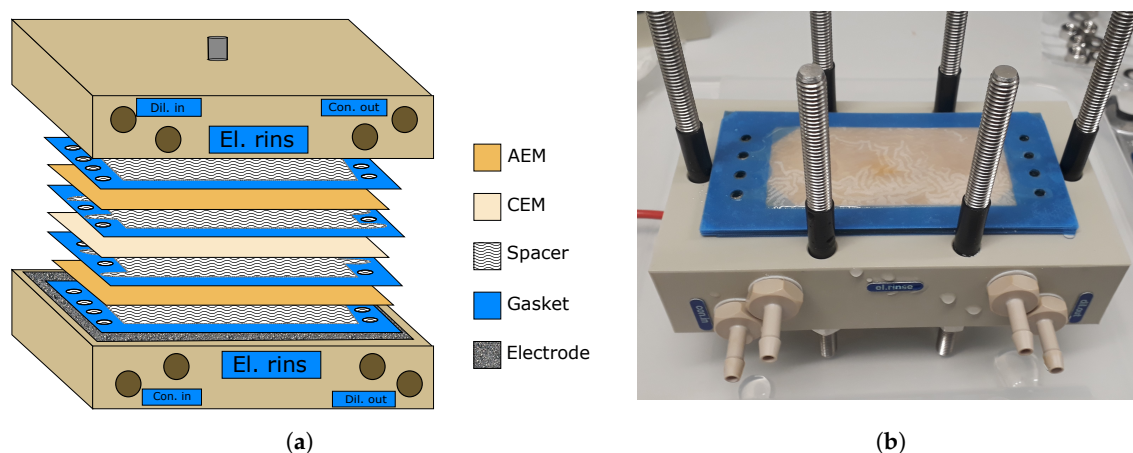


Figure 6. The figure shows the Reverse electrodiolysis (RED) stack used for all stack experiments sketched in (a) and photographed in (b). The holes on the front of the stack are the inlet and outlet of the dilute solution, the concentrated solution and the electrode rinse (redox) solution. In the experiments, nine cell pairs were used (ten AEM and nine CEM).

The dilute and concentrated solutions were pumped in through two separate openings at the endplate. Two holes for each of the solutions (four in total) distribute the solution over the membrane area, where the dilute and the concentrated solutions are distributed in every second compartment. Both solutions flow out from the cell through two holes in the other end plate (see Figure 6). The redox solution is pumped in at each electrode and flows out from the same electrode to avoid short-circuiting by circulating the redox solution. The redox couple used in the experiments was a solution of FeCl_2 (0.5 M), FeCl_3 (0.5 M) and NaCl (1.0 M). When the cell was not in use, dilute (0.05–0.5 M) NaCl solution was pumped in at all compartments, including the redox compartment.

To reduce the loss in temperature between the heated inlet solutions and the flow channels inside the RED stack, the RED stack and the tubing were kept in a heating cabinet throughout the measurements at 40 °C. The temperature was measured in the inlet salt solutions and at the outlet solution. The temperature was kept within 40 ± 1 °C.

Linear sweep voltammetry (LSV) [41] (p. 178) was run for each concentration and temperature. In all LSV experiments reported in this work, scan rates of 5 mV s^{-1} were used. From these experiments, the current and voltage were recorded directly using a Gamry Interface 5000E potentiostat.

Chronopotentiometry measurements of the cells containing the electrodes, the redox solution and one AEM were carried out to compensate for the voltage losses at the electrode. The current steps were held for 1000 s and randomised. Between every current step, the current was set to zero for 100 s. At the end of every step, resistance was found from dividing the measured voltage by the set current. The resistance was plotted versus the current density to find the ohmic region and its ohmic resistance, R_{blank} . The unit cell voltage was found from the following:

$$E_{\text{uc}} = \frac{E_{\text{total}} - R_{\text{blank}}I}{N}, \quad (17)$$

where E_{total} is the total stack voltage; R_{blank} is the resistance of wires, electrodes, redox solution and one AEM; I is the current; and N is number of unit cells (not including the last AEM).

3.4. Life-Cycle Analysis

An energy storage capacity of 1 GWh for the EESS is considered, which is 20% of the daily energy needed for 100,000 Norwegian households (every house using a total of 20 MWh per year [42]). The energy storage capacity of the EESS is defined by the amount of NaCl solution available. In every cubic meter of concentrated salt solution, there is 15 MJ, or 4.2 kWh, of available energy relative to a cubic meter of a dilute salt solution [3], meaning two tanks of $2.4 \cdot 10^5 \text{ m}^3$ with NaCl solution are needed: one for the dilute and one for the concentrated solution. Operating within 90% of the state of charge is considered. The energy is assumed to be used during 2 h in the evening (duck curve [7]), with an energy to power ratio (E2P) of 2. The power density needed is defined by the number of unit cells and the total membrane area, where the power needed from the RED stack is 0.5 GW (E2P = 2). The power density from the RED stack is found from measurements and can be used to find the total membrane area and the end-plate area (from the number of unit cells). The materials considered in the life-cycle inventory for the production of EESS are detailed in Table 3. The base scenario considers polyamide 6.6 (PA 6.6) as spacer material; however, polyamide 6 (PA 6), polyethylene terephthalate (PET) and polypropylene (PP) were also analysed (see Table 3). The GW (kg CO₂ equivalents) per kg produced material and the CED (Wh) per kg for all the materials included in the EESS is given in Table 3.

Table 3. Materials used in an EESS (1 GWh storage capacity).

Component	Material	Density	GW kg CO ₂ eq./kg	CED kWh/kg
Salt solution	NaCl	2.525 mol L ⁻¹ *	0.305	1.14
Redox solution	FeCl ₂	0.5 mol L ⁻¹	0.300	1.19
Redox solution	FeCl ₃	0.5 mol L ⁻¹	0.642	2.53
Gasket	Polyvinylchloride	1380 kg m ⁻³	2.03	16.9
CEM	Cationic resin	1100 kg m ⁻³	1.88	10.7
AEM	Anionic resin	1100 kg m ⁻³	3.60	17.6
Electrode	Graphite	2000 kg m ⁻³	2.29	15.0
End-plate	Aluminium scrap	2700 kg m ⁻³	0.833	0.155
Water	DI water	1000 kg m ⁻³	9.92·10 ⁻⁴	5.39·10 ⁻³
Tank	Lean concrete	2300 kg m ⁻³	0.0753	0.106
Spacer	Polyamide 6.6	1140 kg m ⁻³	6.74	38.5
	Polyamide 6	1130 kg m ⁻³	9.88	34.3
	Polyethylene terephthalate	1350 kg m ⁻³	3.28	22.0
	Polypropylene	905 kg m ⁻³	2.18	21.2

* mean value of the concentrated and dilute concentration.

The parameters for the LCA of the EESS are given in Table 4. The table includes results from the measurements and calculations.

Table 4. Parameters considered in the inventory of EESS (1 GWh storage capacity).

Name	Value
General	
Usable capacity	1 GWh *
Discharging time	2 h *
Operation time	20 years *
Available energy in NaCl solutions	4167 Wh m ⁻³ [3]
Water tanks	
Total storage capacity needed ^a	10 GWh ***
Volume water tanks	2.4·10 ⁶ m ³ ***
Number of tanks	2 *
Height	100 m *
Radius	276 m ***
Wall thickness	0.30 m *
RED Stack	
Power density needed (E2P=2)	0.5 GW ***
Number of unit cells	500 *
Height flow channel	155 μm **
Height redox channel	155 μm **
Porosity flow channel	1
Thickness membrane	50 μm **
Thickness electrode	3.5 mm *
Thickness endplate	0.05 m *
Power density per membrane area RED	1 W m ² **
Total membrane area needed	5.00·10 ⁸ m ² ***
Cell area needed ($A_{mem.}/2N_{uc}$)	5.00·10 ⁵ m ² ***
Volume redox solution	155 m ³ ***
Volume NaCl solution in cell	7.75·10 ⁴ m ³ ***

* set, ** measured, *** calculated, ^a considering 90% of state of change.

4. Results and Discussion

This section contains all the experimental results from permselectivity and stack measurements, where the results are compared with modelled data. An LCA of the EESS is included at the end.

4.1. Permselectivity

The measured permselectivity at room temperature (23 °C) for AEM (FAS-50) and CEM (FKS-50) is given in Figure 7.

The measured permselectivity is in the same range as given in the literature: Daniilidis et al. [43] measured a mean permselectivity of 0.8 and 0.7 for concentration ratios 0.050 M/5.0 M and 0.55 M/4.5 M, respectively. Daniilidis, referring to Veerman et al. [44], pointed out that the losses from co-ion transport increase with increasing concentration difference. An increase in the concentration difference will also increase the counterion transport, increasing the permselectivity. However, the data obtained here cannot be used to deduce the two transport numbers separately.

The permselectivity of CEM is higher than for AEM, as expected, partly due to a higher amount of fixed charges in CEM than in AEM, reducing the number of co-ions in the CEM.

Due to a constant mean concentration between the compartments in every experiment, the salt transport number can be assumed constant. Given the measured permselectivity in Figure 7, and salt transport numbers given in Equation (5) (0.8 for AEM and 0.9 for CEM), the water transport number is as given in Table 5. The large uncertainty in the permselectivity leads to large uncertainty in the transport numbers. Zlotorowicz et al. [10] found the water transport number to be 8 ± 7 and 6 ± 1 for two similar membranes from Fumatech but at lower concentrations.

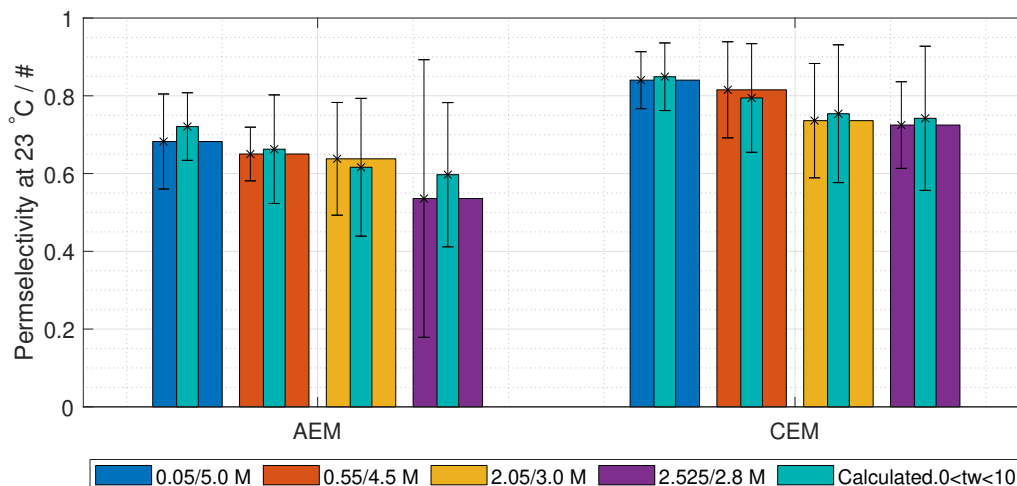


Figure 7. Measured permselectivity of AEM and CEM at 23 °C with 0.95 confidence interval, together with the modelled permselectivity (Equation (3)), with water transport number equal to 5 (error bars with water transport number of 0 and 10) and salt transport numbers equal to Długolecki et al. [15] (see Equation (5)).

Table 5. Transport number of water in Fumatech membranes FAS-50 and FKS-50 given salt transport numbers from Equation (5) and measured permselectivities given in Figure 7.

Concentration/M/M	0.05000/5.000	0.5500/4.500	2.050/3.000	2.525/2.800
t_w AEM	5 ± 7	4 ± 2	4 ± 4	6 ± 9
t_w CEM	5 ± 4	4 ± 4	5 ± 4	5 ± 3

Smaller concentration differences need to be evaluated to find the exact contribution from the water and salt transport number on the permselectivity [10]. However, in this work, the aim is to find the permselectivity at operating conditions.

4.2. Stack Measurements

The resistance of a blank cell with one AEM and redox solution is shown in Figure 8, where the ohmic resistance of the blank cell is $3 \cdot 10^{-3} \Omega m^2$. At an absolute current density lower than $30 A m^{-2}$, the non-ohmic losses are negligible. As shown later, the operational current density of the full RED/ED stack is mainly in the ohmic region and a constant resistance is subtracted.

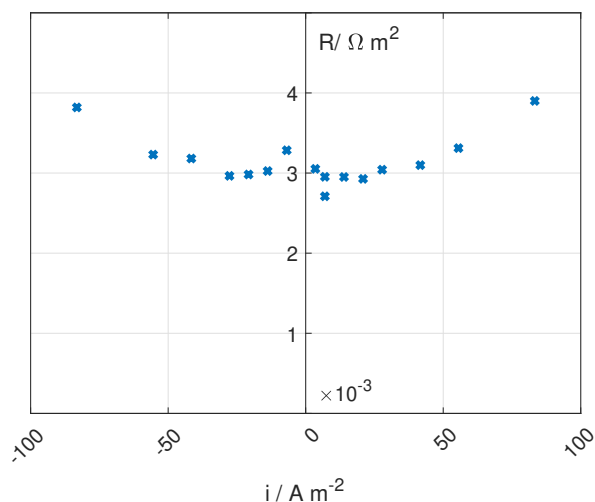


Figure 8. Resistance of the blank RED cell with one AEM and redox solution at 25 °C.

The polarisation curves for the EESS stack measurements are given in Figure 9. The unit cell potential given in the graph is calculated from Equation (17).

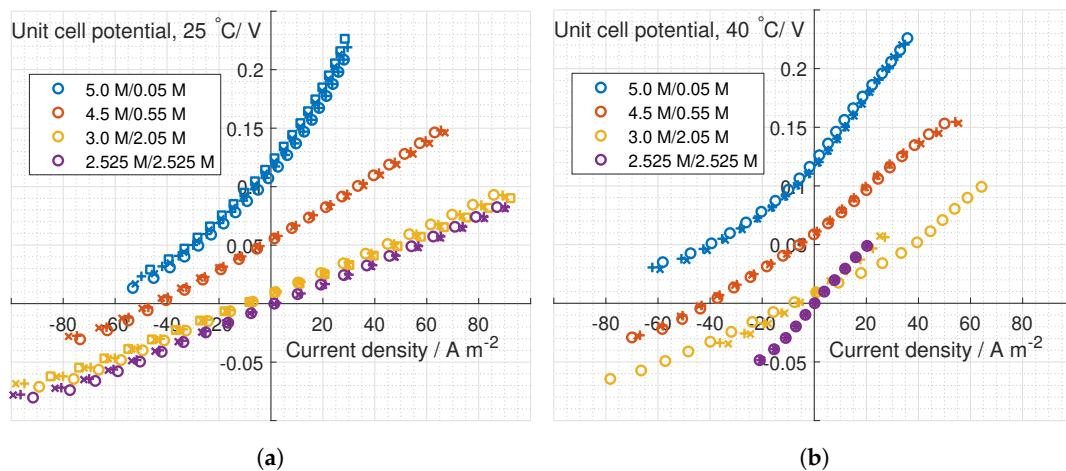


Figure 9. Polarisation curves for all measurements obtained at 25 °C (a) and at 40 °C (b). Markers □, ○, + and x of same colour indicate reproducibility of a given experiment.

The OCV of the RED-stack gained from Figure 9 is plotted in Figure 10a together with the calculated potential from Equation (2) (with $\alpha = 1$) and the OCV from the permselectivity measurements. The unit cell resistance (R_{blank} subtracted), together with the calculated resistance, is given in Figure 10b.

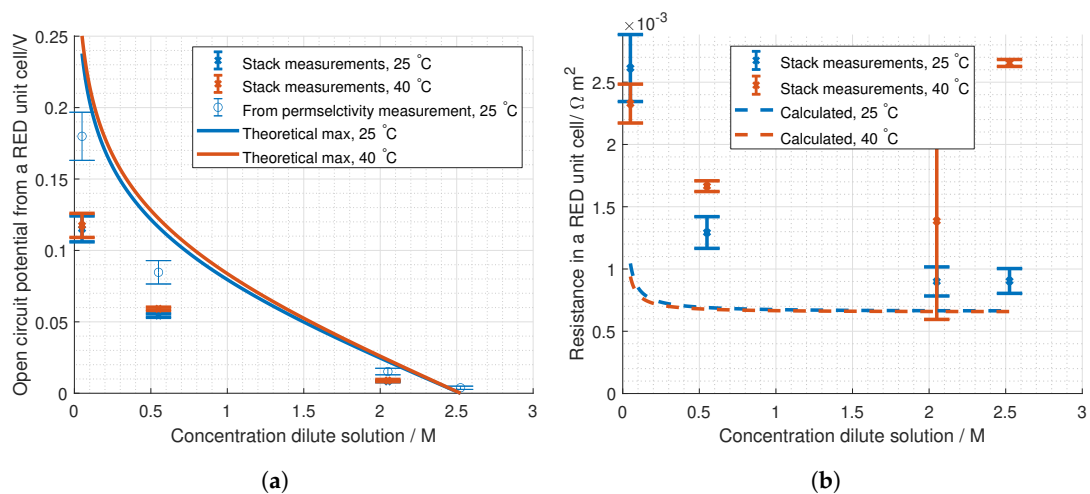


Figure 10. (a) Experimental open-circuit voltage (OCV) for one unit cell (dots) and calculated, theoretical OCV from Equation (2) (solid lines), compared to dilute concentration. (b) Measured unit cell resistances (dots) with the evaluated, calculated unit resistance from Equation (12) (dashed line), compared to dilute concentration. $c_c = 5.05 - c_d$.

The theoretical OCV ($\alpha = 1$) is two times as high as the measured OCV. One of the reasons is the drop in the permselectivity mentioned in Section 4.1. Tedesco et al. [45] and Daniilidis et al. [43] also measured half of the theoretical potential using similar concentrations for the concentrated feed as in our experiments.

The low OCV from the stack measurements compared to the calculated OCV with the measured permselectivities can also be due to concentration polarisation. The solutions were stirred during the permselectivity measurements, while the flow in the cell was low to keep the pumping losses down.

The measured resistance is higher than the calculated resistance. The membrane resistance used in the calculation is obtained from the Fumatech datasheet [13,14]. This value is representative for 0.5 M NaCl, while the mean concentration is 2.525 M in the experiments conducted in this work. Conductivity measurements carried out on FAS-50 and FKS-50 soaked in up to 4.3 mol kg⁻¹ NaCl, indicating a decrease in conductivity with increasing mean concentration. For FAS-50, the conductivity decreased from 4 to 2 mS cm⁻¹ from 0.9 to 4.3 M in concentration at 23 °C and from 8 to 3 mS cm⁻¹ at 40 °C. The conductivity in FKS-50 decreased from 2 to 1 mS cm⁻¹ from 0.9 to 1.8 M and from 4 to 1 mS cm⁻¹ from 0.9 to 1.8 M at 40 °C [5]. These measurements indicate that the calculated resistance in Figure 10b is too low.

The cell resistance (mostly) increases with decreasing dilute concentration due to the decrease in the resistance of the dilute flow compartment. Jalili et al. [46] simulated the resistance in the flow compartments in RED using OpenFOAM, where they found the resistance to be 0.4 mΩ m² and 0.04 mΩ m² for the dilute and concentrated solutions, respectively. These calculations are similar to our total calculated resistance. At 40 °C, the unit cell resistance decrease from 0.05000 M to 0.5500 M. The measured stack resistance at 40 °C for 2.525 M/2.525 M is high compared to the other resistances at 40 °C, where this irregularity was not detected during measurements. This could be due to oxidation and precipitation of the iron in the redox solution. This could also have affected the measurements at a dilute concentration of 2.05 M and could be the reason for the high uncertainty.

The ohmic losses can be reduced by decreasing the compartment thickness, where 100 μm or lower is recommended by Vermaas et al. [47]. Increasing the temperature would also decrease the resistance of the solutions [5]. Jalili et al. showed a significant decrease in stack resistance, increasing the temperature from 10 °C to 80 °C. However, for the temperature range used in the present study, Jalili et al. [7] did not show a prominent change in stack resistance, where the stack resistance was measured to be between 1 and 2 mΩ m² between 25 °C and 40 °C. It is also worth mentioning that the model in Reference [7] uses concentrations 0.01 M to 1.0 M. However, both the study by Jalili et al. [7] and our work show that membranes with lower resistance should be prioritised, especially at high concentration difference and temperature.

The polarisation curves in Figure 9 show dominating ohmic losses in the galvanostatic region where the EESS is discharged. At higher current densities in the galvanostatic region (and in the super galvanostatic region), some losses due to electrode kinetics can also be observed. At the electrolytic region, where the EESS is charged, the losses are mainly ohmic, with some losses from the mass transfer, particularly for the higher concentration differences.

The kinetic losses can be reduced by increasing the temperature [48] (p. 200). In the experiments carried out in this work, only the sodium chloride solutions were heated and not the redox solution due to increased oxidation and precipitation of the iron at elevated temperature. Increasing the temperature of the redox solution could be done in a sealed container with nitrogen or argon bubbled into it. The mass transport losses can be reduced by increasing the mixing achieved by increasing the volumetric flow of the solution. This will, however, increase the pumping losses.

The power density gained from RED, the power density used in ED (given a charging current half the discharging current) and the corresponding current density at maximum power are given in Table 6 (together with a 95% confidence interval).

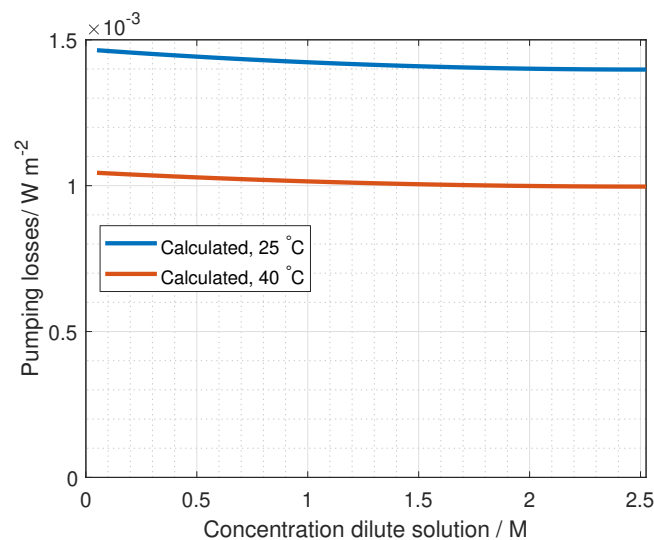
The maximum power density per unit cell (uc) area from discharging the EESS is 1.5 ± 0.3 W m_{uc}⁻² and 2.0 ± 0.3 W m_{uc}⁻² at 25 °C and 40 °C respectively. The charging energy, given half the discharging current, is 2.1 ± 0.3 W m_{uc}⁻² and 3.8 ± 0.9 W m_{uc}⁻² at 25 °C and 40 °C respectively.

The discharge power density for Egmond et al. [9] was approximately 0.5 W m⁻², 0.7 W m⁻² and 0.7 W m⁻² for 10 °C, 25 °C and 40 °C respectively at a discharge current density of 15 A m⁻². Daniilidis et al. [43] measured power density from RED between 3.8 and 6.7 W m⁻² from 25 to 60 °C respectively, with solutions of 0.01 M and 5 M. Daniilidis used membranes from Neosepta and Tokuyama Inc. which had a mean permselectivity of almost 0.8 at maximum concentration difference.

Table 6. Peak power current density, peak power density and charging power density at different temperatures and different concentrations fractions.

c_c/c_d	25 °C			40 °C		
	$i_{\text{dischar.}}$	$p_{\text{max}}^{\text{dischar.}}$	$p^{\text{char.}}$	$i_{\text{dischar.}}$	$p_{\text{max}}^{\text{dischar.}}$	$p^{\text{char.}}$
M/M	A m ⁻²	W m _{uc} ⁻²	W m _{uc} ⁻²	A m ⁻²	W m _{uc} ⁻²	W m _{uc} ⁻²
5.000/0.05000	28 ± 3	1.5 ± 0.2	2.1 ± 0.3	42 ± 7	2.0 ± 0.3	3.8 ± 0.9
4.500/0.5500	22 ± 1	0.60 ± 0.08	0.76 ± 0.07	21 ± 2	0.58 ± 0.02	0.8 ± 0.1
3.000/2.050	4.8 ± 0.8	0.020 ± 0.003	0.024 ± 0.006	3 ± 2	0.015 ± 0.008	0.019 ± 0.009
2.525/2.525	0.8 ± 0.2	(5 ± 3)·10 ⁻⁴	(6 ± 4)·10 ⁻⁴	0.08 ± 0.09	(1.2 ± 0.4)·10 ⁻⁵	(2.2 ± 2.1)·10 ⁻⁵

The modelled power lost in pumping is presented in Figure 11. The concentration impact on the pumping power is small (4.5% at both 25 °C and 40 °C) while the temperature has a significant impact; the losses decrease by 29% when raising the temperature from 25 °C to 40 °C. The efficiency for the charging and discharging EESS, together with the total energy storage efficiency, is given in Table 7. As seen from Table 6, Figure 11 and Table 7, the pumping losses are negligible compared to the power density output from EESS at the higher concentration ratios.

**Figure 11.** The power density lost in pumping. $C_c = 5.05 - C_d$.**Table 7.** The efficiency of ED, RED and ED/RED.

c_c/c_d M/M	25 °C			40 °C		
	η_{ED} (max = 0.8)	η_{RED} (max = 0.5)	$\eta_{\text{ED/RED}}$ (max = 0.4)	η_{ED} (max = 0.8)	η_{RED} (max = 0.5)	$\eta_{\text{ED/RED}}$ (max = 0.4)
5.000/0.05000	0.74 ± 0.16	0.47 ± 0.10	0.34 ± 0.11	0.65 ± 0.21	0.40 ± 0.10	0.26 ± 0.11
4.500/0.5500	0.79 ± 0.10	0.50 ± 0.08	0.39 ± 0.08	0.75 ± 0.14	0.48 ± 0.04	0.36 ± 0.07
3.000/2.050	0.76 ± 0.22	0.47 ± 0.11	0.36 ± 0.13	0.78 ± 0.54	0.47 ± 0.34	0.36 ± 0.37
2.525/2.525	0.27 ± 0.17	0	0	0.013 ± 0.009	0	0

As seen from Table 7, the efficiency of discharging the EESS is between 0.40 and 0.50, compared to the reversible potential ($\eta_{\text{RED,max}} = 0.5$). Below the concentration ratio 3.000 M/2.050 M, the pumping losses are higher than the power output, and according to this study, the battery should not be operated below this concentration limit. At 3.000 M/2.050 M and higher ratios, the power density shows no significant variation with concentration ratio. The deviation from 0.5 can be explained by pumping

power and kinetic losses. As seen from Figure 9, the kinetic losses are highest at the concentration ratio 5.000 M/0.05000 M and 40 °C.

There is no significant change in efficiency with temperature indicating a proportional change in the available energy with the measured energy. Earlier studies by Jalili et al. [7] show an impact from the temperature on efficiency. However, the temperature range in the study by Jalili et al. is larger than the one given here. Daniilidis et al. [43] found an energy efficiency of 15–20% at the same concentration difference as that used in our experiments, where the efficiency decreased with temperature from 20% to below 10% from 10 °C to 60 °C. However, Daniilidis et al. [43] used a fixed current for all their experiments.

4.3. Energy Price and Membrane Cost

The energy cost of the EESS needs to be competitive with local energy prices to be adapted into the market. However, as explained in Jalili et al. [7], one can also be paid to dump surplus electricity, as is seen in Europe. However, in this work, the energy price of EESS will be compared with the energy price in the EU and USA.

A financial feasibility study by Daniilidis [43] found that the most influential parameter on the RED power plant cost is the price of the membranes. A Nafion 117 membrane is a popular IEM and costs approximately 1.2 \$ cm⁻² [49] (12,000 \$ m⁻²), while the membranes from Fumatech cost approximately 0.05 \$ cm⁻² (500 \$ m⁻²) at lab scale. However, Raka et al. [6] have estimated a drop in the price of IEMs given increased production rate. For simplicity and an initial estimate, only the cost of the membranes is included in our analysis.

The lifetime for the system is assumed to vary from 3 to 10 years [50,51], with 3% downtime [43] and a discharging duration of 3 h per day (duck-curve). The peak power density from EESS at 40 °C is taken from Table 6. The energy price from an EESS is estimated and shown in relation to the membrane cost in Figure 12.

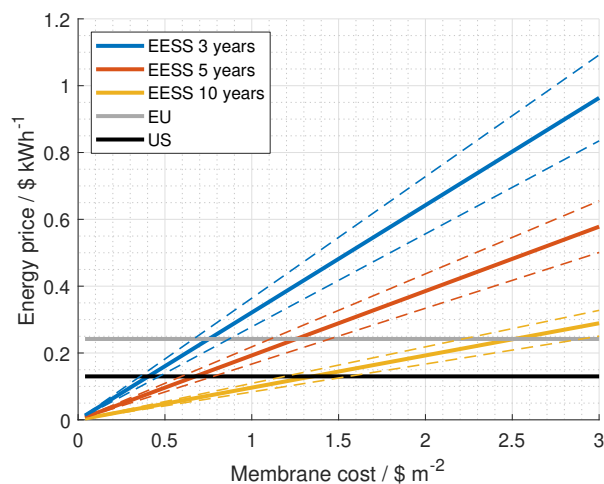


Figure 12. Cost of electric energy generation (\$/kWh) using the EESS at 40 °C with 95% confidence interval from measured power density (dotted lines) and 3-, 5- and 10-year lifetimes, compared to the energy price in the EU and USA.

The average energy prices are 0.24 \$ kWh⁻¹ and 0.13 \$ kWh⁻¹ in the EU [52] and the USA [53], respectively. To generate electricity below these prices using EESS with an operational time of 5 years (three hours per day and 3% downtime), considering power densities given in Table 6 at 40 °C, the membrane cost needs to be lower than 1.3 ± 0.2 \$ m⁻² and 0.67 ± 0.08 \$ m⁻² for the EU and the USA respectively. If the membrane lifetime increases to 10 years, the price can be 2.5 ± 0.3 \$ m⁻² and 1.4 ± 0.2 \$ m⁻² to compete with the energy price in the EU and the USA respectively.

4.4. Life-Cycle Analysis

The total mass of each material needed for building a full-scale EESS is given in Table 8.

Table 8. Inventory (material used per functional unit (1 MWh) of EESS).

Name	Mass per Energy Stored kg/MWh
NaCl	$7.11 \cdot 10^5$
FeCl ₂	12.6
FeCl ₃	9.82
End-plate	$1.35 \cdot 10^5$
Gasket	30.3
IEM	$2.75 \cdot 10^4$
DI water	$4.62 \cdot 10^6$
Electrode	$7.00 \cdot 10^3$
Tank	$2.40 \cdot 10^7$
Spacer materials	
PA6.6	$1.42 \cdot 10^4$
PA6	$1.40 \cdot 10^4$
PET	$1.68 \cdot 10^4$
PP	$1.12 \cdot 10^4$

The impact on GW and the CED is calculated from multiplying the data given in Table 8 with the data given in Table 3. The impacts for the base scenario, using PA6.6 for the spacer, is given in Figure 13.

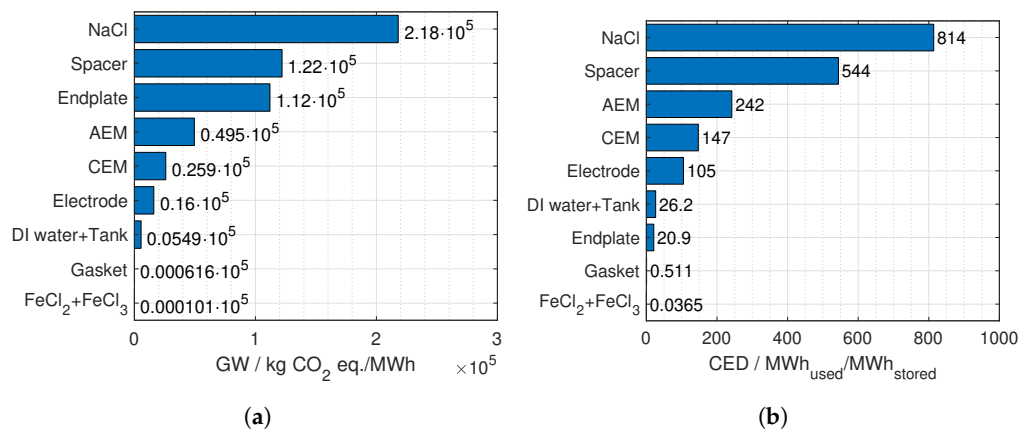


Figure 13. Impact on GW (kg CO₂ eq./MWh) (a) and the CED (MWh/MWh) (b) for each component in the production phase.

The most significant impact on both GW and CED is the NaCl, 40% and 42% respectively, followed by the spacer material with a contribution of 23% and 29% respectively. Some of the NaCl (and DI water) can be substituted by brine water, which is included in the SimaPro database. However, this alternative was omitted due to lack of information on the brine water concentration in the database. Another solution is to decompress and heat seawater or brine water (see Reference [5]) and to therefore make the solution more concentrated. However, the LCA of this process is an option for future work.

The spacer has more possibilities for variations. Four different spacers are included to compare their total GW and CED. This is given in Figure 14. The best material to use for the spacer is polypropylene (PP) with a reduction of 17% in GW and 15% in CED compare to the base scenario (PA 6.6).

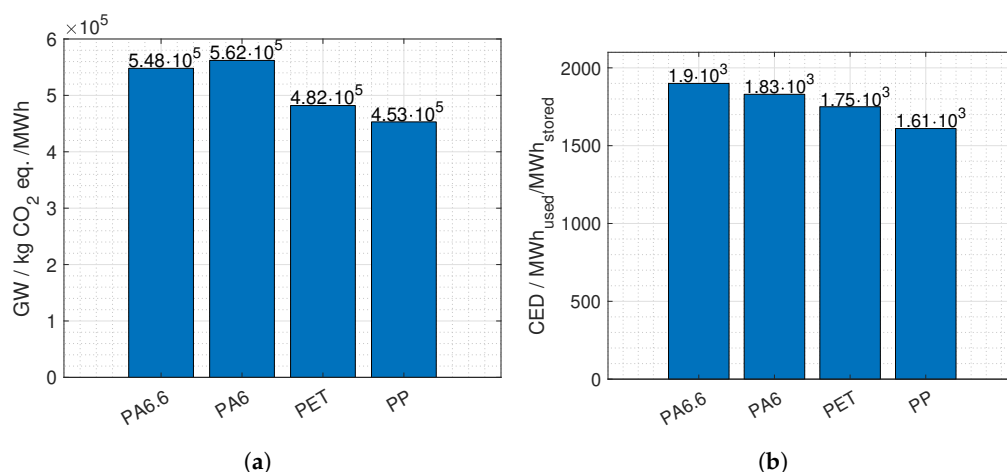


Figure 14. Impact on GW (kg CO₂ eq./MWh) (a) and the CED (MWh/MWh) (b) for the total production phase using four different spacer materials.

The environmental footprint of EESS was compared to Li-ion batteries considering the same functional unit and system boundary (only production phase). Many LCAs of Li-ion batteries are conducted (e.g., References [54–57]), reporting on GW factors between 17,000–356,000 kg CO₂ eq. per MWh capacity. The large variation originated from the different assumption on energy demand for cell manufacturing and the amount of material needed [57]. If the use phase is considered in the system boundary, the life span needs to be included. Three years of operation life span for the Li-ion battery is assumed in many studies [58–60], resulting in a GW impact between 16 and 333 kg CO₂ eq./MWh. However, an EESS has the potential for a longer use phase with an estimation of 20 years of life span. This will result in a GW of 62 kg CO₂ eq./MWh for EESS, which is in the range of the GW factor of the Li-ion battery. Given these assumption of life span, one would need more than 6 Li-ion batteries to match the lifetime of an EESS. The CED for Li-ion batteries is reported to range between 267 and 580 MWh/MWh [54]. However, if we again consider the different life spans, the CED is between 0.24 t and 0.55 MWh/MWh for Li-ion (three years of life span) and 0.22 MWh/MWh (for 20 years of life span) for EESS. Thus, the CED for EESS is lower than the CED for Li-ion batteries when the LCA includes the production and use phase.

5. Conclusions

Reverse electro dialysis and electro dialysis can be combined into an EESS, where the system is charged by increasing the concentration difference between two salt solutions and is discharged by mixing the same two salt solutions through alternating AEMs and CEMs. Given this system as a closed system, the concentrations can be higher than the naturally occurring concentration.

Permselectivities of one AEM and one CEM from Fumatech were measured at NaCl concentrations close to saturation. The mean permselectivity decreased from 0.95 using seawater to a mean permselectivity ranging from 0.6 to 0.8 using concentration ratios from 2.800 M/2.525 M to 5.000 M/0.05000 M, indicating a higher co-ion transport with the counterions and/or water transport in the membranes.

Stack measurements of a RED/ED cell were conducted, measuring the current density and voltage. The OCV at 5.000 M/0.05000 M was measured to 115 ± 9 mV and 118 ± 8 mV at 25 °C and 40 °C respectively. The measured OCV was 50% of the theoretical ($\alpha = 1$) and 60% of the calculated OCV using the measured permselectivities.

The power density from EESS was measured to 1.5 ± 0.2 W m⁻² and 2.0 ± 0.3 W m⁻² at 25 °C and 40 °C respectively. The efficiency was 0.4 for the higher concentration differences while the system was found to use more energy than gained for concentration ratios below 3.000 M/2.050 M. The temperature impact on the OCV and power density were not significant in this study, showing the need for raising the temperature above 40 °C in future studies to potentially show a temperature

dependency. The main objective is to increase the permselectivity of the membranes and to reduce their ionic resistance.

A simple cost analysis of the energy production is conducted given the EESS power density measured in this work. For a lifetime of 5 years, three hours of operation per day and 3% downtime, the membrane price needs to be lower than $1.3 \pm 0.2 \text{ \$ m}^{-2}$ and $0.67 \pm 0.08 \text{ \$ m}^{-2}$ to match the energy price in the EU and the USA, respectively. Given a lifetime of 10 years, the price can be $2.5 \pm 0.3 \text{ \$ m}^{-2}$ and $1.4 \pm 0.2 \text{ \$ m}^{-2}$ to compete with the energy price in the EU and the USA, respectively.

An LCA of EESS with total energy storage capacities of 1 GWh per day, 1 W power per membrane area and a lifetime of 20 years, gives a GW factor of 62 kg CO₂ eq. per MWh and a CED of 0.22 MWh/MWh for the production phase of the EESS. This study indicates that the mass of CO₂ eq. released in the production phase per MWh storage capacity using EESS is similar to the mass of CO₂ eq. per MWh released from Li-ion battery production. The CED per MWh capacity in EESS is in the lower range of the CED from large scale Li-ion storage.

Author Contributions: K.W.K. measured the membrane permselectivity and potential from the RED stack, did all the calculations and simulations and has contributed to the LCA of the RED system. K.W.K. has written the article with contributions from weekly supervision meetings. M.M. did the LCA in SimaPro and contributed to the writing of the LCA part of the manuscript. R.B. contributed with scientific feedback, copyedited the article and joined many of the weekly meetings. F.S. contributed with guidance in electrochemistry and general measurements at the lab. F.S. has also contributed with discussions at many of the weekly meetings. K.E.E. and O.S.B. formulated the idea of combining RED and ED to an energy storage system and to use waste-heat to increase its efficiency. They guided K.W.K. in the measurements and theory, guided weekly meetings, and contributed with scientific feedback and otherwise advised manuscript development for editorial level of proofreading. All authors have read and agreed to the published version of the manuscript.

Funding: The Research Council of Norway (project No: 267989) and NTNU (project No: 68024012) is greatly acknowledged for the financial aid of this project.

Acknowledgments: Financial support from the Norwegian University of Science and Technology (NTNU) via PhD grants and strategic research program ENERSENSE (Energy and Sensor Systems) is greatly acknowledged. We thank Kristina Lopez Hatlen, Eilif Sommer Øyre, Markus Solberg Wahl and Olivier Bernard for useful discussions on stack development, temperature regulations and LCA.

Conflicts of Interest: The authors declare no conflicts of interest.

Abbreviations

The following abbreviations are used in this manuscript:

AEM	anion exchange membrane
CDP	capacitive Donnan potential
CED	cumulative energy demand
CEM	cation exchange membrane
ED	electrodialysis
EESS	electrodialytic energy storage system
GW	global warming
IEM	ion exchange membrane
LCA	life-cycle analysis
LCI	life-cycle inventory
LSV	linear sweep voltammetry
MCDI	membrane capacitive deionisation
OCV	open-circuit voltage
PRO	pressure retarded osmosis
RED	reverse electrodialysis
RO	reverse osmosis
SGES(S)	salinity gradient energy storage (system)

Appendix A. The Apparent Permselectivity

Generally, we define the apparent permselectivity as a ratio between observed potential and chemical potential:

$$\alpha = \frac{E_{\text{measured}}}{-\frac{\Delta\mu_s}{F}}. \quad (\text{A1})$$

In measuring these potentials, there is a need for a framework describing the electroosmotic coupling (between charge and water). Therefore, we turn to nonequilibrium thermodynamics.

For any monovalent salt (AC dissolving as A^- and C^+), nonequilibrium thermodynamics define the following flux–force relations:

$$J_s = -L_{ss} \frac{d\mu_s}{ds} - L_{sw} \frac{d\mu_w}{dx} - L_{s\phi} \frac{d\phi}{dx} \quad (\text{A2})$$

$$J_w = -L_{ws} \frac{d\mu_s}{ds} - L_{ww} \frac{d\mu_w}{dx} - L_{w\phi} \frac{d\phi}{dx} \quad (\text{A3})$$

$$j = -L_{\phi s} \frac{d\mu_s}{ds} - L_{\phi w} \frac{d\mu_w}{dx} - L_{\phi\phi} \frac{d\phi}{dx}. \quad (\text{A4})$$

In understanding the origin of the apparent permselectivity, it is natural to start with Equation (A4) at zero current ($j = 0$), yet from the concept of the electromotoric force, we can still observe the potentials and their linkage to each other. At open circuit ($j = 0$) and by dividing by $L_{\phi\phi}$, we get

$$\frac{d\phi}{dx} = -\frac{L_{\phi s}}{L_{\phi\phi}} \frac{d\mu_s}{ds} - \frac{L_{\phi w}}{L_{\phi\phi}} \frac{d\mu_w}{dx}. \quad (\text{A5})$$

The term $\frac{L_{\phi s}}{L_{\phi\phi}}$ expresses the amount of moles transported per coulomb (moles of electrons), and likewise, the expression $\frac{L_{\phi w}}{L_{\phi\phi}}$ expresses the moles of water transported per coulomb. Turning to the first expression, we by definition have

$$t_s \equiv F \frac{L_{\phi s}}{L_{\phi\phi}} \quad (\text{A6})$$

and exemplifying for cationic exchange membranes

$$t_{s,\text{CEM}} = t_{C^+} - t_{A^-} = 2t_{C^+} - 1. \quad (\text{A7})$$

For cationic exchange membranes; if the cationic transference number, t_{C^+} , is 1, then one mole of salt is transferred per coulomb. If the cationic transference number, t_{C^+} , is 0.5, no net transport of the salt takes place as a current passes. If the cationic transference number, t_{C^+} , is 0.95, then per 100 coulomb, 95 cations are moved one way and 5 anions the other way so that 0.9 moles of salt is transferred per coulomb and t_s becomes 0.9. For the transference of water,

$$t_w \equiv F \frac{L_{\phi w}}{L_{\phi\phi}} \quad (\text{A8})$$

which is related to the electroosmotic drag or water transferred per ion and, sometimes, the hydration shell. When t_s is 1, then t_w is the amount of water dragged along per cation. The value of this is often reported to be in the range of 5 to 10 in water solutions but can be smaller in a membrane, which is why we use 5 ± 5 when modelling permselectivity in Figure 7. When the salt transport number, t_s , is lower than 1, the water electromotoric transference number is lower because water is dragged back due to anions (sticking to the example of CEM) moving in the opposite direction. When modelling this, one can use the relation in Equation (A15) to describe the dependency between

apparent permselectivity and salt concentration. Inserting Equations (A6) and (A8) into Equation (A5), we get

$$\frac{d\phi}{dx} = -\frac{t_s}{F} \frac{d\mu_s}{dx} - \frac{t_w}{F} \frac{d\mu_w}{dx}. \quad (\text{A9})$$

The Gibbs–Duhem equation states that

$$\sum_{i=s,w} N_i d\mu_i = -SdT + VdP \quad (\text{A10})$$

and at constant temperature and pressure and when dividing by the mass of the solution, we get $d\mu_w = -\frac{m_s}{m_w} d\mu_s$. By inserting into Equation (A9), we get

$$d\phi = -\frac{t_s}{F} d\mu_s + \frac{t_w}{F} \frac{m_s}{m_w} d\mu_s. \quad (\text{A11})$$

We then introduce the partial chemical potential of the salt

$$d\mu_s = 2RT d\ln[m_s \gamma_s] = 2RT (d\ln[m_s] + d\ln[\gamma_s]) = RT \left(\frac{dm_s}{m_s} + \frac{d\gamma_s}{\gamma_s} \right). \quad (\text{A12})$$

By inserting Equation (A12) into (A11), we get generally

$$d\phi = -\frac{2RT}{F} (t_s d\ln[m_s \gamma_s] - t_w M_w (dm_s + m_s d\ln[\gamma_s])) \quad (\text{A13})$$

where $m_w^{-1} = M_w / \rho_w$, the density of water, ρ_w is close to one and where M_w is the molar mass of water. By integration we obtain

$$\Delta\phi = -\frac{2RT}{F} (t_s \Delta\ln[m_s \gamma_s] - t_w M_w (\Delta m_s + m_s \Delta\ln[\gamma_s])) \quad (\text{A14})$$

where the term $(\Delta m_s + m_s \Delta\ln[\gamma_s])$ can be simplified to Δm_s for the system considered here. This stems from a few practical considerations. When comparing the first term, Δm_s , to the second term, $m_s \Delta\ln[\gamma_s]$, in light of the activity coefficient plotted in Figure 4, where we can see that, under the constraint that the sum of the two concentrations is always 5 (from the charging principle), the ratio of the two activity coefficients is almost always between 0.9 and 1.1; $\Delta\ln[\gamma_s]$ is always ± 0.1 . Doing this, one will find that the term Δm_s is always ten times $m_s \Delta\ln[\gamma_s]$. Since additionally, t_w has an uncertainty of around $\pm 50\%$, we carry through with the simplification that $(\Delta m_s + m_s \Delta\ln[\gamma_s]) \approx \Delta m_s$. The challenge with these two terms stems from introducing the Gibbs–Duhem Equation, where we introduce m_s and m_w as constants next to the differential of the chemical potential of the salt when they really are variables; when we have two concentrations, it becomes unclear which of the two solutions m_s relates to when calculating the apparent permselectivity, α .

Considering that the apparent permselectivity is defined by the observed potential difference (or modelled by nonequilibrium thermodynamics) $\Delta\phi_m$ divided by the theoretical and uncoupled one, $\Delta\phi_{\text{theor}}$, we get

$$\alpha = \frac{\Delta\phi_m}{\Delta\phi_{\text{theor}}} = \frac{-\frac{2RT}{F} (t_s \Delta\ln[m_s \gamma_s] - t_w M_w \Delta m_s)}{-\frac{2RT}{F} \Delta\ln[m_s \gamma_s]} \quad (\text{A15})$$

$$\alpha = \left(t_s - t_w M_w \frac{\Delta m_s}{\Delta\ln[m_s \gamma_s]} \right)$$

Equation (A15) is always true (at zero current). However, when two concentrations are near each other (say the ratio is between 0.6 or 1.4), Equation (A13) becomes

$$d\phi = -\frac{2RT}{F} [t_s d\ln[m_s \gamma_s] - t_w M_s m_s (d\ln[m_s] + d\ln[\gamma])] \quad (\text{A16})$$

where m_s can be equal to either of the solutions or the average, given the uncertainties of the water transference number, and Equation (A15) becomes

$$\alpha = (t_s - t_w M_w m_s) \quad (\text{A17})$$

Although Equation (A17) is only valid when the two concentrations are similar to each other, it offers a simple explanation on the ratio between the apparent permselectivity and ambient concentration derived from a thermodynamic point, otherwise not possible. That is, if the membrane have the same selectivity independent of ambient solution concentration (and several membranes do), the apparent permselectivity can be expected to decrease as the concentration increases.

References

1. DNV-GL. Energy Transition Outlook 2019; Technical report, DNV-GL; 2019. Available online: <https://eto.dnvgl.com/2019/index.html> (accessed on 15 January 2020).
2. Sholkovitz, E.R. Flocculation of dissolved organic and inorganic matter during the mixing of river water and seawater. *Geochim. Cosmochim. Acta* **1976**, *40*, 831–845. [CrossRef]
3. Boon, N.; Van Roij, R. Blue energy from ion adsorption and electrode charging in sea and river water. *Mol. Phys.* **2011**, *109*, 1229–1241. [CrossRef]
4. Pattle, R.E. Production of electric power by mixing fresh and salt water in the hydroelectric pile. *Nature* **1954**, *174*, 660. [CrossRef]
5. Krakhella, K.W.; Bock, R.; Burheim, O.S.; Seland, F.; Einarsrud, K.E. Heat to H₂: Using Waste Heat for Hydrogen Production through Reverse Electrodialysis. *Energies* **2019**, *12*, 3428. [CrossRef]
6. Raka, Y.D.; Karoliussen, H.; Lien, K.M.; Burheim, O.S. Opportunities and challenges for thermally driven hydrogen production using reverse electrodialysis system. *Int. J. Hydrog. Energy* **2020**, *45*, 1212–1225. [CrossRef]
7. Jalili, Z.; Krakhella, K.W.; Einarsrud, K.E.; Burheim, O.S. Energy generation and storage by salinity gradient power: A model-based assessment. *J. Energy Storage* **2019**, *24*, 100755. [CrossRef]
8. Kingsbury, R.S.; Chu, K.; Coronell, O. Energy storage by reversible electrodialysis: The concentration battery. *J. Membr. Sci.* **2015**, *495*, 502–516. [CrossRef]
9. van Egmond, W.J.; Starke, U.K.; Saakes, M.; Buisman, C.J.N.; Hamelers, H.V.M. Energy efficiency of a concentration gradient flow battery at elevated temperatures. *J. Power Sour.* **2017**, *340*, 71–79. [CrossRef]
10. Zlotorowicz, A.; Strand, R.V.; Burheim, O.S.; Wilhelmsen.; Kjelstrup, S. The permselectivity and water transference number of ion exchange membranes in reverse electrodialysis. *J. Membr. Sci.* **2017**, *523*, 402–408. [CrossRef]
11. Cipollina, A.; Micale, G. *Sustainable Energy from Salinity Gradients*; Woodhead Publishing: Sawston, UK, 2016.
12. Kamcev, J.; Paul, D.R.; Manning, G.S.; Freeman, B.D. Ion diffusion coefficients in ion exchange membranes: Significance of counterion condensation. *Macromolecules* **2018**, *51*, 5519–5529. [CrossRef]
13. FuelCellStore. *Fumasep FKS-50*; 2019. Available online: <https://fuelcellstore.com/spec-sheets/fumasep-fks-50-technical-specifications.pdf> (accessed on 15 January 2018).
14. FuelCellStore. *Fumasep FAS-50*; 2019. Available online: <https://fuelcellstore.com/spec-sheets/fumasep-fas-50-technical-specifications.pdf> (accessed on 15 January 2018).
15. Długolecki, P.; Anet, B.; Metz, S.J.; Nijmeijer, K.; Wessling, M. Transport limitations in ion exchange membranes at low salt concentrations. *J. Membr. Sci.* **2010**, *346*, 163–171. [CrossRef]
16. Giorno, L.; Drioli, E.; Strathmann, H. *Water Transport in Ion-Exchange Membranes*; Springer: Berlin/Heidelberg, Germany, 2016; pp. 2011–2015. [CrossRef]
17. Pitzer, K.S.; Pabalan, R.T. Thermodynamics of NaCl in steam. *Geochim. Cosmochim. Acta* **1986**, *50*, 1445–1454. [CrossRef]

18. Larchet, C.; Auclair, B.; Nikonenko, V. Approximate evaluation of water transport number in ion-exchange membranes. *Electrochim. Acta* **2004**, *49*, 1711–1717. [[CrossRef](#)]
19. Stokes, R.H.; Robinson, R.A. Ionic hydration and activity in electrolyte solutions. *J. Am. Chem. Soc.* **1948**, *70*, 1870–1878. [[CrossRef](#)]
20. Glueckauf, E. The influence of ionic hydration on activity coefficients in concentrated electrolyte solutions. *Trans. Faraday Soc.* **1955**, *51*, 1235–1244. [[CrossRef](#)]
21. Pytkowicz, R. *Activity Coefficients in Electrolyte Solutions*; CRC Press: Boca Raton, FL, USA, 1979.
22. Ribeiro, A.C.; Lobo, V.M.; Burrows, H.D.; Valente, A.J.; Sobral, A.J.; Amado, A.M.; Santos, C.I.; Estes, M.A. Mean distance of closest approach of potassium, cesium and rubidium ions in aqueous solutions: Experimental and theoretical calculations. *J. Mol. Liq.* **2009**, *146*, 69–73. [[CrossRef](#)]
23. Malmberg, C.G.; Maryott, A.A. Dielectric constant of water from 0 °C to 100 °C. *J. Res. Natl. Bur. Stand.* **1956**, *56*, 1–8. [[CrossRef](#)]
24. Miyawaki, O.; Saito, A.; Matsuo, T.; Nakamura, K. Activity and activity coefficient of water in aqueous solutions and their relationships with solution structure parameters. *Biosci. Biotechnol. Biochem.* **1997**, *61*, 466–469. [[CrossRef](#)]
25. Afanasiev, V.N.; Ustinov, A.N.; Vashurina, I.Y. State of Hydration Shells of Sodium Chloride in Aqueous Solutions in a Wide Concentration Range at 273.15–373.15 K. *J. Phys. Chem. B* **2008**, *113*, 212–223. [[CrossRef](#)]
26. Onori, G. Ionic hydration in sodium chloride solutions. *J. Chem. Phys.* **1988**, *89*, 510–516. [[CrossRef](#)]
27. Ramon, G.Z.; Feinberg, B.J.; Hoek, E.M.V. Membrane-based production of salinity-gradient power. *Energy Environ. Sci.* **2011**, *4*, 4423. [[CrossRef](#)]
28. Post, J.W.; Hamelers, H.V.M.; Buisman, C.J.N. Energy recovery from controlled mixing salt and fresh water with a reverse electrodialysis system. *Environ. Sci. Technol.* **2008**, *42*, 5785–5790. [[CrossRef](#)] [[PubMed](#)]
29. Długołęcki, P.; Gambier, A.; Nijmeijer, K.; Wessling, M. Practical potential of reverse electrodialysis as process for sustainable energy generation. *Environ. Sci. Technol.* **2009**, *43*, 6888–6894. [[CrossRef](#)] [[PubMed](#)]
30. EXW Foxboro. Conductivity Ordering Guide. 1999. Available online: https://www.academia.edu/17588429/Conductivity_v_Concentration (accessed on 20 January 2019).
31. Hamann, C.H.; Hamnett, A.; Vielstich, W. *Electrochemistry*; Wiley-VCH: Cambridge, MA, USA, 1998.
32. Schlumberger. *Resistivity of NaCl Solutions*; Technical report; Schlumberger: Houston, TX, USA, 2017.
33. Arvidsson, R.; Tillman, A.M.; Sandén, B.A.; Janssen, M.; Nordelöf, A.; Kushnir, D.; Molander, S. Environmental assessment of emerging technologies: recommendations for prospective LCA. *J. Ind. Ecol.* **2018**, *22*, 1286–1294. [[CrossRef](#)]
34. Ecoinvent. Allocation Cut-off by Classification. 2019. Available online: <https://www.ecoinvent.org/database/system-models-in-ecoinvent-3/cut-off-system-model/allocation-cut-off-by-classification.html> (accessed on 20 July 2019).
35. Climate Change Connection. CO₂ Equivalents. 2016. Available online: <https://climatechangeconnection.org/emissions/co2-equivalents/> (accessed on 13 April 2019).
36. Huijbregts, M.; Steinmann, Z.; Elshout, P.; Stam, G.; Verones, F.; Vieira, M.; Hollander, A.; Zijp, M.; van Zelm, R. *ReCiPe 2016 v1.1*; Technical report; National Institute for Public Health and the Environment: Utrecht, The Netherlands, 2017. Available online: https://www.pre-sustainability.com/download/Report_ReCiPe_2017.pdf (accessed on 13 April 2019).
37. Althaus, H.J.; Bauer, C.; Doka, G.; Dones, R.; Hischier, R.; Hellweg, S.; Humbert, S.; Köllner, T.; Loerincik, Y.; Margni, M.; et al. *Implementation of Life Cycle Impact Assessment Methods—Data v2.0 (2007)*; Technical report; Swiss Centre for Life Cycle Inventories: Dübendorf, Switzerland, 2007.
38. Fumatech. *Membrane Module Fumatech ED-40 for Research Studies in the Field of Electro-Membrane Processes*; Technical report; Fumatech: Bietigheim-Bissingen, Germany, 2020.
39. Marlow. Material Properties. 2019. Available online: <https://www.marlowropes.com/material-properties> (accessed on 20 July 2019).
40. Burheim, O.S.; Seland, F.; Pharoah, J.G.; Kjelstrup, S. Improved electrode systems for reverse electro-dialysis and electro-dialysis. *Desalination* **2012**, *285*, 147–152. [[CrossRef](#)]
41. Pletcher, D.; Greff, R.; Peat, R.; Peter, L.M.; Robinson, J.; Derek, R. *Instrumental Methods in Electrochemistry*; Elsevier: Amsterdam, The Netherlands, 2001.
42. SSB—Ann Christin Bøeng. *Energy Consumption in Households, 2012*; 2014. Available online: <https://www.ssb.no/en/statbank/table/10574/tableViewLayout1/> (accessed on 14 March 2019).

43. Daniilidis, A.; Vermaas, D.A.; Herber, R.; Nijmeijer, K. Experimentally obtainable energy from mixing river water, seawater or brines with reverse electrodialysis. *Renew. Energy* **2014**, *64*, 123–131. [CrossRef]
44. Veerman, J.; De Jong, R.M.; Saakes, M.; Metz, S.J.; Harmsen, G.J. Reverse electrodialysis: Comparison of six commercial membrane pairs on the thermodynamic efficiency and power density. *J. Membr. Sci.* **2009**, *343*, 7–15. [CrossRef]
45. Tedesco, M.; Brauns, E.; Cipollina, A.; Micale, G.; Modica, P.; Russo, G.; Helsen, J. Reverse electrodialysis with saline waters and concentrated brines: a laboratory investigation towards technology scale-up. *J. Membr. Sci.* **2015**, *492*, 9–20. [CrossRef]
46. Jalili, Z.; Burheim, O.S.; Einarsrud, K.E. New insights into computational fluid dynamic modeling of the resistivity and overpotential in reverse electrodialysis. *ECS Trans.* **2018**, *85*, 129–144. [CrossRef]
47. Vermaas, D.A.; Saakes, M.; Nijmeijer, K. Doubled power density from salinity gradients at reduced intermembrane distance. *Environ. Sci. Technol.* **2011**, *45*, 7089–7095. [CrossRef]
48. Oldham, K.; Myland, J.; Bond, A. *Electrochemical Science and Technology: Fundamentals and Applications*; John Wiley & Sons: Hoboken, NJ, USA, 2011.
49. Nafion Westerling Perfluorinated Membrane. Available online: <http://www.sigmaaldrich.com/catalog/product/aldrich/274674?lang=en®ion=NO> (accessed on 4 February 2020).
50. Post, J.W.; Goeting, C.H.; Valk, J.; Goinga, S.; Veerman, J.; Hamelers, H.V.M.; Hack, P.J.F.M. Towards implementation of reverse electrodialysis for power generation from salinity gradients. *Desalin. Water Treat.* **2010**, *16*, 182–193. [CrossRef]
51. Turek, M.; Bandura, B. Renewable energy by reverse electrodialysis. *Desalination* **2007**, *205*, 67–74. [CrossRef]
52. Electricity Price Statistics. Available online: https://ec.europa.eu/eurostat/statistics-explained/index.php/Electricity_price_statistics (accessed on 4 February 2020).
53. Electric Sales, Revenue, and Average Price (TableT5.a). Available online: https://www.eia.gov/electricity/sales_revenue_price/ (accessed on 5 February 2020).
54. Arvidsson, R.; Janssen, M.; Svanström, M.; Johansson, P.; Sandén, B.A. Energy use and climate change improvements of Li/S batteries based on life cycle assessment. *J. Power Sour.* **2018**, *383*, 87–92. [CrossRef]
55. Samaras, C.; Meisterling, K. *Life Cycle Assessment of Greenhouse Gas Emissions from Plug-in Hybrid Vehicles: Implications for Policy—Supporting Online Information*; ACS Publications: Washington, DC, USA, 2008.
56. Kim, H.C.; Wallington, T.J.; Arsenault, R.; Bae, C.; Ahn, S.; Lee, J. Cradle-to-gate emissions from a commercial electric vehicle Li-ion battery: A comparative analysis. *Environ. Sci. Technol.* **2016**, *50*, 7715–7722. [CrossRef] [PubMed]
57. Ellingsen, L.A.W.; Hung, C.R.; Strømman, A.H. Identifying key assumptions and differences in life cycle assessment studies of lithium-ion traction batteries with focus on greenhouse gas emissions. *Transp. Res. Part D Transp. Environ.* **2017**, *55*, 82–90. [CrossRef]
58. Battery University. How to Prolong Lithium-Based Batteries. 2019. Available online: https://batteryuniversity.com/learn/article/how_to_prolong_lithium_based_batteries (accessed on 15 April 2019).
59. Tektronix, Inc. *Lithium-Ion Battery Maintenance Guidelines*; Tektronix, Inc.: Beaverton, OR, USA, 2004. Available online: <https://www.tek.com/document/technical-brief/lithium-ion-battery-maintenance-guidelines> (accessed on 15 April 2019).
60. Carter, R.; Cruden, A.; Hall, P.J. Optimizing for efficiency or battery life in a battery/supercapacitor electric vehicle *IEEE Trans. Veh. Technol.* **2012**, *61*, 1526–1533. [CrossRef]

